Lifetime measurements in ^{92}Mo: Investigation of seniority conservation in the $N = 50$ isotones

M. Ley,* L. Knafla, J. Jolie, A. Esmaylzadeh, A. Harter, A. Blazhev, C. Fransen, A. Pfeil, and J.-M. Régis
Institut für Kernphysik, Universität zu Köln, D-50937 Köln, Germany

P. Van Isacker
Grand Accélérateur National d'Ions Lourds, CEA/DRF–CNRS/IN2P3, Bvd Henri Becquerel, F-14076 Caen, France

(Received 11 September 2023; accepted 9 November 2023; published 22 December 2023)

Excited states in the yrast and negative parity bands in ^{92}Mo were populated in two different experiments using the ^{90}Zr$(\alpha, 2n)^{92}$Mo and ^{93}Nb$(p, 2n)^{92}$Mo fusion-evaporation reactions at the Cologne FN Tandem accelerator and measured using a hybrid setup of high purity germanium and lanthanum bromide detectors. Lifetimes of the excited 2_1^+, 4_1^+, 6_1^+, 8_1^+, 5_1^-, 7_1^-, and 9_1^- states were measured using the γ-γ fast-timing technique. The newly measured lifetime of the 4_1^+ state differs from the recently published value measured using the recoil distance Doppler shift method. Experimental $B(E2)$ strengths of excited states in ^{92}Mo are used to predict theoretical $B(E2)$ values in the $N = 50$ isotones from ^{93}Tc up to ^{95}Rh using semiempirical calculations in the single-j orbital $0g_{9/2}$ for the protons.

DOI: 10.1103/PhysRevC.108.064313

I. INTRODUCTION

The semimagic $N = 50$ isotones between ^{90}Zr and the doubly magic ^{100}Sn are of particular interest to test the nuclear shell model (SM) since in this region the valence protons gradually fill the $0g_{9/2}$ orbital above an energetically separated, closed core. Consequently, the low energy nuclear structure in this region can be assumed to originate from the interaction of protons confined to the $0g_{9/2}$ orbital. This implies the use of the concept of seniority to describe the low-spin structure ($J \leqslant 8$) of these nuclei. Seniority was first introduced by Racah to describe pairing interaction of electrons in the atom [1]. For a fermionic system of n identical particles, which all have the same angular momentum j and interact through a pairing force, seniority υ is a conserved quantum number and defined as the number of particles that do not pairwise couple to angular momentum $J = 0$ [1]. In nuclear physics, the validity of seniority symmetry has also been demonstrated for a broader class of empirical nucleon-nucleon interactions [2–5] and is expected to provide a useful description for a variety of regions of the nuclear chart [6]. Seniority is strictly conserved for systems with $j \leqslant 7/2$ [7] but is usually relatively well conserved among identical nucleons, even if $j > 7/2$ [8,9]. Recent studies found indications for a partial seniority conservation [10] as well as seniority-breaking behavior [11–13] for protons in the $0g_{9/2}$ orbital. Seniority conservation and breaking remains a topic of current interest in this region of the nuclear chart.

The single-j approximation applied in this article uses the experimentally determined quadrupole transition strength from the two-nucleon j^2 system (^{92}Mo) to make analytical predictions for the quadrupole transition strength in the j^n systems of the isotonic chain, up to ^{95}Rh. This *ansatz* already proved to be successful in the similar case of protons in the $0h_{9/2}$ orbital in the region above ^{208}Pb [14]. Relations between $B(E2)$ values in the j^2 and j^n systems can be derived in general. Such relations become analytical if seniority is conserved and therefore deviations from the analytical relations may provide important information on the question of seniority conservation.

In order to have an adequate basis for the single-j prediction, lifetimes of the first excited states in ^{92}Mo, especially of the 4_1^+ state, were measured with high precision using the fast-timing method with two independent experiments.

II. EXPERIMENT

The two independent experiments used different nuclear reactions to populate excited states in ^{92}Mo. In the first experiment, the states were populated using a ^{90}Zr$(\alpha, 2n)^{92}$Mo fusion evaporation reaction, it will be referred to as EXP1 in the following. The 5.3 mg/cm^2 thick target of 97.62% enriched ^{90}Zr was irradiated with a beam of 27 MeV α particles provided by the Cologne 10 MV FN Tandem accelerator with an average current of 3 pnA. Due to a clean reaction channel, almost no other nuclei were populated, and hence no major contaminations are visible in the γ-ray spectrum. The setup consisted of eight high purity germanium (Ge) detectors and nine $LaBr_3$(Ce) detectors (hereafter denoted as LaBr). Six of the LaBr detectors were actively shielded with bismuth germanium oxide (BGO) anti-Compton shields. The remaining LaBr detectors were passively shielded against scattered γ rays using lead sheaths. A 500 MHz digitizer, implementing online interpolation constant fraction discrimination (CFD), was used to record time and pulse height information from

*Corresponding author: mley@ikp.uni-koeln.de

the LaBr detectors photomultipliers (PM). A detailed investigation of the digital CFDs for fast-timing experiments is given in Ref. [15].

In the second experiment (EXP2), excited states in ^{92}Mo were populated using a ^{93}Nb$(p, 2n)^{92}$Mo reaction. The target was 5.4 mg/cm^2 of monoisotopic ^{93}Nb and the proton beam had an energy of 18 MeV. In both cases the targets were solid and thick enough to stop all reaction residues. The stopping times are much shorter than the lifetimes measured with the fast-timing technique. Both experiments were performed using the HORUS spectrometer fast-timing configuration [16–19]. Notably, the second experiment was performed almost one year later and the exact positions of the detectors differ between the two configurations. The two data sets yield strictly independent results.

Using the fast-timing method, lifetimes of excited states are deduced by measuring the time difference between the observation of events that indicates the population and depopulation of the state. Here, these events are γ rays populating and depopulating the state of interest. The fast-timing method is sensitive down to the range of picoseconds [20,21]. Lifetimes that are significantly larger than the time resolution of the fast-timing setup can be extracted by fitting the exponential tail of the time spectrum or using the convolution method [20,22]. For lifetimes in the range of the setups time resolution and smaller, the centroid shift method [23] is used. The method is based on measuring the centroid of the time distribution, mathematically also referred to as the first moment, to deduce the lifetime.

To extract the signals time information, a fast 500 MHz digitizer with an implemented real-time interpolating CFD algorithm was used to provide time stamps with picosecond precision [15]. In this way the data are intrinsically symmetrical with regard to the interchange of the start and stop detectors and therefore, an easy creation of symmetrical energy-energy-time-difference cubes for the analysis is possible. In the following, only aspects of the fast-timing method that are relevant to the presented analysis will be discussed. For more details on the fast-timing method in general, please refer to Refs. [21,24] and for the analysis using symmetrical fast-timing cubes as done in this study, please refer to Refs. [15,25].

A time difference spectrum for a given feeder-decay cascade is created by gating on the respective transitions. The lifetime τ results from the spectrum as the shift of the distribution's centroid C, corrected for the energy-dependent γ-γ time walk (TW) of the respective feeder-decay combination

$$C = \tau + TW(E_{\text{feeder}}, E_{\text{decay}}), \quad (1)$$

$$TW(E_{\text{feeder}}, E_{\text{decay}}) = TW(E_{\text{feeder}}) - TW(E_{\text{decay}}). \quad (2)$$

The energy dependence of the time walk was determined experimentally using the standard calibration procedure with a ^{152}Eu source [15,26], which covers a wide range of suitable transition energies and well-known lifetimes of intermediate states. From the measured centroid of the time distribution, for a given feeder-decay cascade with intermediate states in ^{152}Gd or ^{152}Sm with well-known lifetime, the time walk can be derived according to Eq. (1). The lifetimes used within the time walk calibration procedure were taken from Ref. [27] and the lifetime from the 2_1^+ in ^{152}Gd from Ref. [28]. Recently, the lifetime of the first excited 2^+ state in ^{152}Gd was remeasure with high precision, reducing its uncertainty by an order of magnitude [28]. This significantly reduces the uncertainty of the time walk calibration using a ^{152}Eu source as calibration standard. Because the γ-ray energies from the 330–773 keV cascade in ^{92}Mo are almost identical to the 344–779 keV cascade in ^{152}Gd, this optimization of the calibration standard significantly reduced the contribution of the time walk to the uncertainty for the lifetime of the 4_1^+ state in ^{92}Mo. The resulting data points are fitted using the function

$$TW(E_\gamma) = \frac{a}{\sqrt{E_\gamma + b}} + E_\gamma^2\, c + E_\gamma\, d + e. \quad (3)$$

The resulting $TW(E_\gamma)$ curves for EXP1 and EXP2 are shown in Figs. 1 and 2, respectively. For both experiments, the

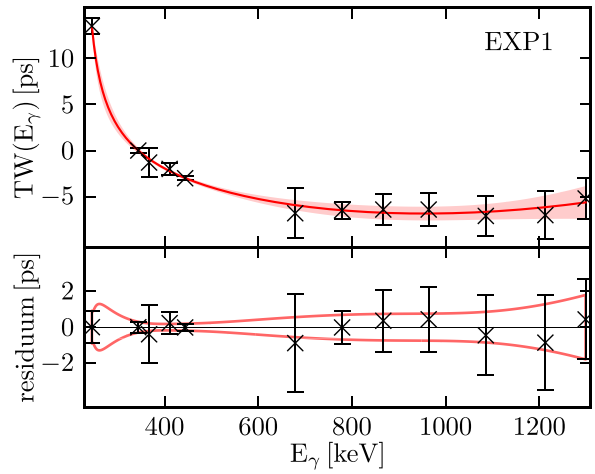

FIG. 1. Calibrated mean time-walk characteristic of the setup used for EXP1 (top). The residuum of the fit and the 1σ uncertainty interval (bottom).

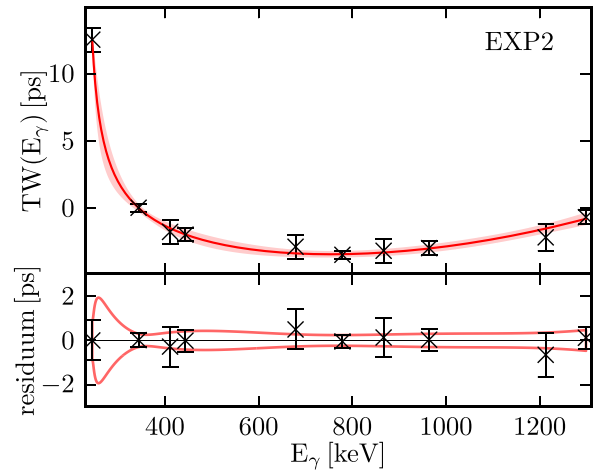

FIG. 2. Calibrated mean time-walk characteristic of the setup used for EXP2 (top). The residuum of the fit and the 1σ uncertainty interval (bottom).

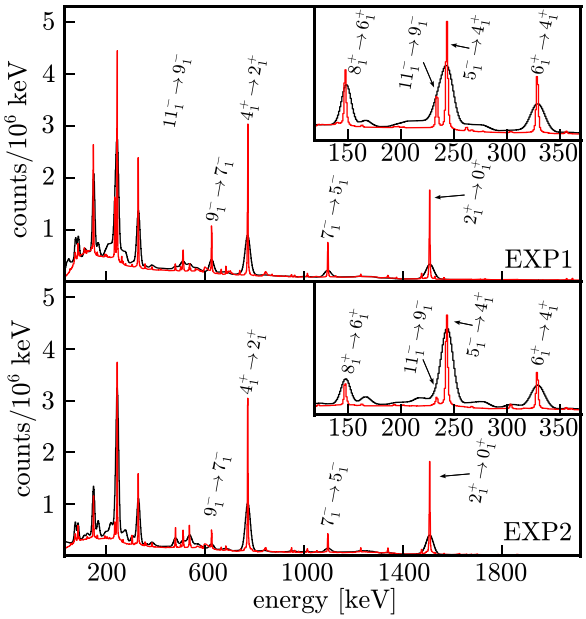

FIG. 3. Coincidence spectra of both experiments for multiplicity three data with Ge-LaBr-LaBr coincidences shown in black and Ge-LaBr-Ge coincidences shown in red. Transitions that were used within the analysis are labeled. The insets show a zoom of the low-energy part.

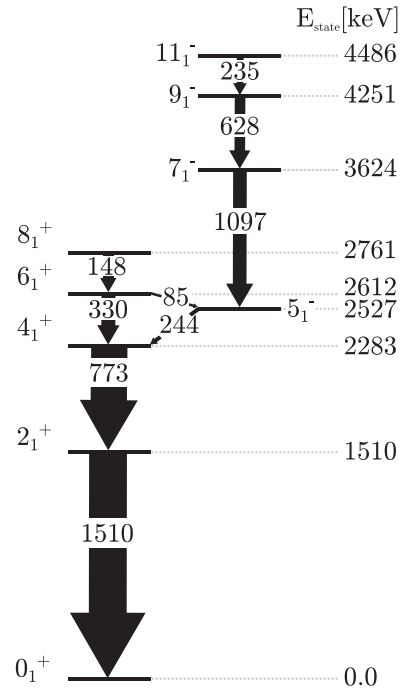

FIG. 4. Partial level scheme showing important states and transitions used within the analysis. The transition energies are given in keV. The arrows thickness approximately emphasize the relative intensities of the transitions observed with the ^{90}Zr(α, $2n$)^{92}Mo reaction (EXP1). Adopted from Refs. [29,30].

maximum range of the time-walk curves amounts to less than 20 ps in the range between 244 and 1299 keV. Coincidence spectra for both experiments are shown in Fig. 3. The spectra are sorted with the coincidence multiplicity condition of one Ge and two LaBr. In both experiments, no significant peaks from nuclei other than ^{92}Mo are visible. Transitions important within the analysis are labeled and Fig. 4 displays a partial level scheme of ^{92}Mo showing the yrast and negative parity bands.

III. ANALYSIS

The lifetimes were extracted from the data using the centroid shift method or by fitting the exponential tail of the time distribution. As an example the procedure for the latter case is shown in Fig. 5 for the lifetimes of the first excited 6_1^+ and 5_1^- states in ^{92}Mo. The lifetime of the 8_1^+ state was determined in the same way but using Ge-LaBr timing. In the following the focus is on the analysis of the lifetime of the 4_1^+ state in ^{92}Mo, which was performed using the centroid shift method. The analyses of the 2_1^+, 7_1^-, and 9_1^- states were performed analogously. For the lifetime analysis of the 4_1^+ state the data were sorted with a threefold coincidence multiplicity condition. Different conditions on the detector types were tested: triples of one Ge and two LaBr and triples of three LaBr with a narrow coincidence window of 20 ns. Taking into account background corrections, which will be discussed in detail later in the text, led to consistent results in all cases. The adopted analysis was done using a threefold multiplicity condition with exactly one Ge and two LaBr detectors. As an example, Figs. 6 and 7 show the resulting LaBr spectra (black) after setting a Ge and a LaBr gate on the feeder (b) or decay (a) transition. To significantly reduce the influence of random correlated γ rays, an additional timing window was placed for the LaBr-LaBr coincidences within the threefold Ge-LaBr-LaBr coincidences. As shown in Ref. [15], for a well-synchronized LaBr array a coincidence window of less

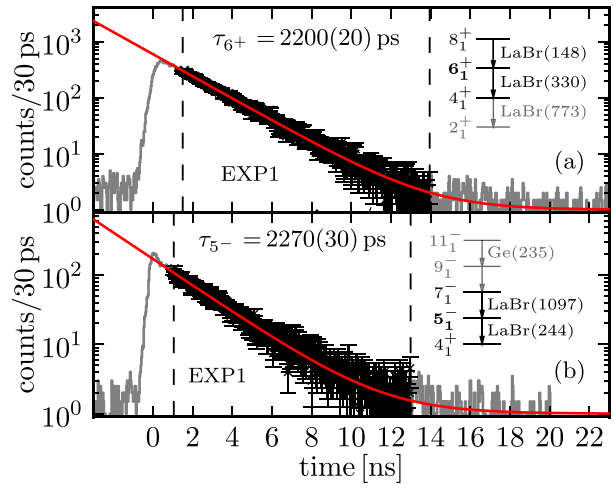

FIG. 5. Time spectra used for the measurement of the lifetime of the 6_1^+ state (a) and for lifetime of the 5_1^- state (b). The procedure is shown for the data from EXP1. The term for the random distributed background was set to a constant value, which was determined via integration and also as parameter from a fit, leading to consistent results. The data from EXP2 was processed in the same way.

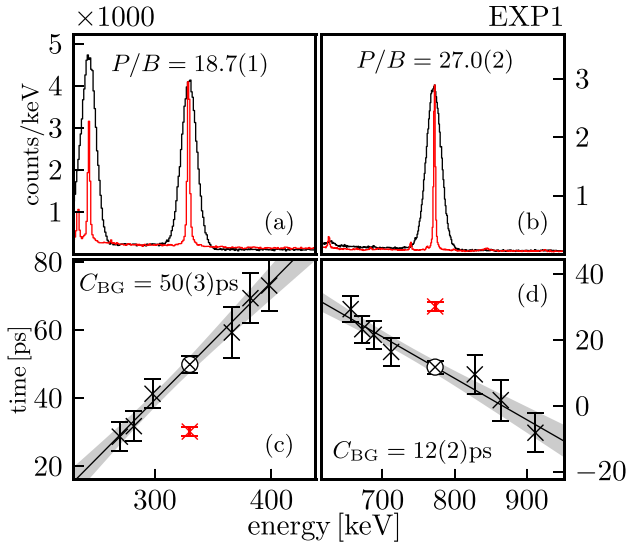

FIG. 6. Background correction procedure for the analysis of the 4_1^+ state measured in EXP1. (a) Resulting spectra after gating on the 773 keV decay transition. (b) Respective spectra after gating on the 330 keV feeder transition. The LaBr spectra are shown in black and corresponding gated Ge spectra for monitoring in red. (c) and (d) The corresponding background interpolation (black), the uncorrected centroid C_{exp} is shown in red, the interpolated centroid C_{BG} is marked with ⊗.

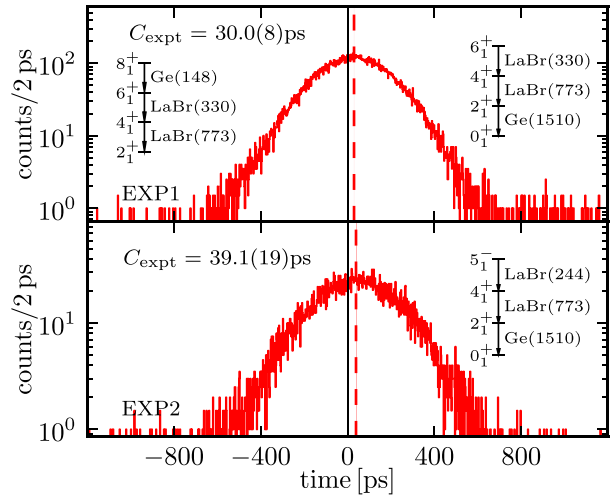

FIG. 8. The resulting time distributions, centroids (dashed lines) and gate information used to measure the 4_1^+ state for EXP1 (top) and EXP2 (bottom). For the upper time distribution, matrices with Ge gates on 148 keV and 1510 keV were added to increase the statistic. Since the multiplicity condition was set to only validate coincidences containing exactly two LaBr hits and one Ge hit the two energy conditions are mutual excluding/exclusive and no risk of double counting exists.

than 10 ns is sufficient for LaBr-LaBr timing. To still gain sufficient coincidences with the Ge detector a large time window of 400 ns was combined with the short LaBr-LaBr timing coincidence window of 10 ns. If such an additional LaBr-LaBr timing window is not applied, the P/B ratios measured in the LaBr spectra will be smaller due to the continuum of random coincidences within the large coincidence window. To verify the absence of contaminating transitions within the broad LaBr peaks, triple events with a coincidence condition for two Ge and one LaBr detectors were built. Using the same gates as before yielded the respective Ge spectra shown in red, which shows no major contamination within the LaBr peaks for the given cascade. The resulting time spectra after setting the second LaBr gate are shown in Fig. 8 together with the resulting centroid of the respective distribution.

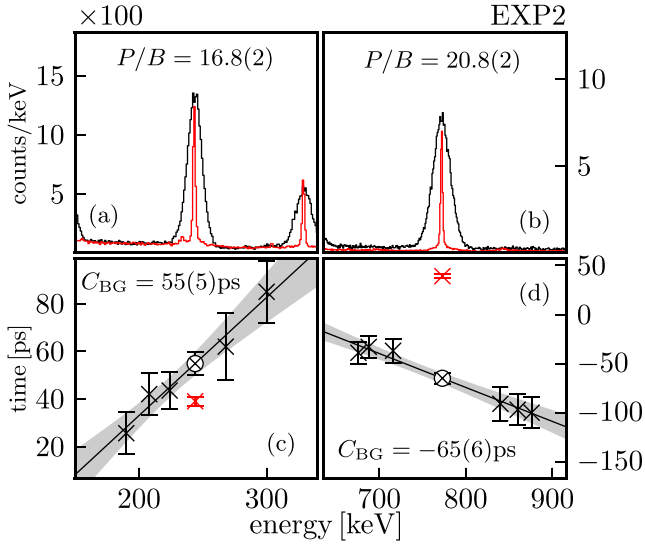

FIG. 7. Background correction procedure for the analysis of the 4_1^+ state measured in EXP2. (a) Resulting spectra after gating on the 773 keV decay transition. (b) Respective spectra after gating on the 244 keV feeder transition. The LaBr spectra are shown in black and corresponding gated Ge spectra for monitoring in red. (c) and (d) The corresponding background interpolation (black), the uncorrected centroid C_{exp} is shown in red, the interpolated centroid C_{BG} is marked with ⊗.

The measured time spectra are always influenced by Compton background beneath the peaks of interest and a background correction procedure was applied. As described in Ref. [26], the centroid of an experimental time-difference distribution is a linear superposition of multiple centroid components and for a proper lifetime determination, the component of the pure peak vs. peak centroid C_{PP} is needed, which was approached by using a background correction procedure as shown in Ref. [26]. The correction is based on Eqs. (4)–(6):

$$C_{PP} = C_{exp} + \tilde{t}_{cor}, \tag{4}$$

$$\tilde{t}_{cor} = \frac{P/B(E_f)\,t_{cor}(E_i) + P/B(E_i)\,t_{cor}(E_f)}{P/B(E_i) + P/B(E_f)}, \tag{5}$$

$$t_{cor} = \frac{C_{exp} - C_{BG}(E)}{P/B(E)}, \tag{6}$$

where C_{BG} is the centroid of the Compton background under the peak and $P/B(E)$ are the respective peak to background ratios. The component C_{BG} is only accessible by interpolating the Compton background in the vicinity of the peak.

TABLE I. Summary of the measured mean lifetimes of the states $J_i^{\pi_i}$ and the respective reduced transition probabilities.

$J_i^{\pi_i} \rightarrow J_f^{\pi_f}$	τ_{EXP1} ps	τ_{EXP2} ps	τ_{adopted} ps	Multipolarity	$B(\sigma\lambda; J_i^{\pi_i} \rightarrow J_f^{\pi_f})$ adopted	$B(\sigma\lambda; J_i^{\pi_i} \rightarrow J_f^{\pi_f})$ literature
$2_1^+ \rightarrow 0_1^+$	$\leqslant 3$	$\leqslant 8$	*$\leqslant 3$*	$E2$	$\geqslant 35\ e^2\,\mathrm{fm}^4$	$207(12)\ e^2\,\mathrm{fm}^4$ [30,31]
$4_1^+ \rightarrow 2_1^+$	22.5(11)	23(2)[a]	*22.5(11)*	$E2$	$132^{+7}_{-6}\ e^2\,\mathrm{fm}^4$	$84.3(14)\ e^2\,\mathrm{fm}^4$ [5]
$6_1^+ \rightarrow 4_1^+$	2200(20)	2220(70)	*2200(20)*	$E2$[b]	$81(2)\ e^2\,\mathrm{fm}^4$	$80(3)\ e^2\,\mathrm{fm}^4$ [30,32]
$\rightarrow 5_1^-$				$E1$[b]	$5.3(6)\times 10^{-5}\ e\,\mathrm{fm}^2$	$5.3(7)\times 10^{-5}\ e\,\mathrm{fm}^2$ [30]
$8_1^+ \rightarrow 6_1^+$	$310(3)\times 10^3$[c]	–	*$310(3)\times 10^3$*	$E2$	$28.6(3)\ e^2\,\mathrm{fm}^4$	$32(1)\ e^2\,\mathrm{fm}^4$ [30,33–37]
$5_1^- \rightarrow 4_1^+$	2270(30)	2250(60)	*2270(30)*	$E1$[d]	$\geqslant 1.88(3)\times 10^{-5}\ e\,\mathrm{fm}^2$	$1.91(5)\times 10^{-5}\ e\,\mathrm{fm}^2$ [30,38]
				$M2$[d]	$\leqslant 93\ \mu N^2\,\mathrm{fm}^4$	$\leqslant 98\ \mu N^2\,\mathrm{fm}^4$ [30]
$7_1^- \rightarrow 5_1^-$	$\leqslant 5$	$\leqslant 7$	*$\leqslant 5$*	$E2$	$\geqslant 101\ e^2\,\mathrm{fm}^4$	–
$9_1^- \rightarrow 7_1^-$	37(11)	29(7)	*31(6)*[e]	$E2$	$271^{+65}_{-44}\ e^2\,\mathrm{fm}^4$	–

[a]Averaged value from feeder-decay cascades 244–773 and 330–773 calculated using a Monte Carlo method.
[b]The branching ratio for the 6_1^+ level was derived using the intensities from Ref. [29].
[c]Determined using Ge-LaBr timing.
[d]Mixing ratio $\delta \leqslant 0.05$ from Ref. [39].
[e]Weighted average from EXP1 and EXP2.

The interpolation of the Compton background is shown in Figs. 6 and 7 (bottom). The results for both experiments are listed in Table I alongside the respective reduced transition probabilities $B(\sigma\lambda)$, which were calculated using the adopted values for the measured lifetimes, decay energies, and the total conversion coefficient calculated using the program BrIcc [40]. The remeasured values for the lifetimes of the 2_1^+, 6_1^+, 5_1^-, and 8_1^+ state fit well to the current literature values. The lifetime of the 4_1^+ state is in significant disagreement with the recently published literature value $\tau_{\mathrm{RDDS}} = 35.5(6)$ ps [5], measured using the recoil distance Doppler shift method and a radioactive beam.

IV. DISCUSSION

The present experimental work established another case of a nucleus with two valence nucleons in a $j = 9/2$ orbital, in which all $B(E2)$ values in the sequence $8_1^+ \rightarrow 6_1^+ \rightarrow 4_1^+ \rightarrow 2_1^+ \rightarrow 0_1^+$ are measured. In a single-j approach the $E2$ transition probabilities in this sequence obey the following rule:

$$B(E2; j^2 J \rightarrow j^2 J-2) = \frac{15(2j+1-J)(2j+2-J)(2j+J)(2j+1+J)(J-1)}{128\pi\, j^2(j+1)^2(2J-1)(2J+1)}\left(N+\frac{3}{2}\right)^2 b^4 e_{\mathrm{eff}}^2, \tag{7}$$

where N is the major oscillator quantum number associated with the j orbital and e_{eff} is the effective charge of the nucleon, which usually is taken the same for all $E2$ transitions in a given nucleus. In Eq. (7) also appears the oscillator length parameter b, for which we use the estimate of Blomqvist and Molinari [41] (see also the more recent discussion of Kirson [42]):

$$b = \sqrt{\frac{41.46}{45A^{-1/3} - 25A^{-2/3}}}\ \mathrm{fm}. \tag{8}$$

It should be stressed that the result (7) is purely geometric, that is, it depends only on the angular momenta involved and not on the interaction between the nucleons. In the column labeled '$\hat{T}_1(E2)$' of Table II, the single-j prediction is compared with the $B(E2)$ values measured in ^{92}Mo. The effective charge in the one-body operator $\hat{T}_1(E2)$ is obtained from the quadrupole moment of the $9/2^+$ ground state of ^{91}Nb, with the experimental value and uncertainty $Q(9/2_1^+) = -25(3)\ e\,\mathrm{fm}^2$. With an oscillator length parameter $b \approx 2.18$ fm this implies $e_{\mathrm{eff}} \approx 1.32$. This effective charge is essentially the same as what is obtained from the $B(E2; 8^+ \rightarrow 6^+)$ value in ^{92}Mo, $e_{\mathrm{eff}} \approx 1.31$. It is possible to obtain better results for ^{92}Mo by fitting the effective charge to the $n = 1$ and $n = 2$ data but that would be problematic given the discrepant description of the $B(E2)$ values in ^{92}Mo.

It is seen from Table II that there are significant deviations from Eq. (7) for all transitions other than $8_1^+ \rightarrow 6_1^+$, in

TABLE II. Experimental and calculated $B(E2)$ values in ^{92}Mo.

υ_i	J_i^π	υ_f	J_f^π	$B(E2; J_i^\pi \rightarrow J_f^\pi)\ (e^2\,\mathrm{fm}^4)$		
				Exp	$\hat{T}_1(E2)$	$\hat{T}_1'(E2)$
2	2_1^+	0	0_1^+	207(12)	89	207(12)
2	4_1^+	2	2_1^+	132^{+7}_{-6}	103	132^{+7}_{-6}
2	6_1^+	2	4_1^+	81(2)	71	81(2)
2	8_1^+	2	6_1^+	28.6(3)	28	28.6(3)

particular for the $2_1^+ \to 0_1^+$ transition. The situation is reminiscent of the one in the $A = 210$ isotopes of lead and polonium but, interestingly, whereas in the latter nuclei the calculated $B(E2; 2_1^+ \to 0_1^+)$ is a factor two larger than the measured value, in ^{92}Mo the single-j prediction is more than a factor two too small.

It is assumed that the correct $B(E2)$ values can be obtained by considering an appropriately large model space, which, when reduced to a manageable model space, gives rise to effective charges. The purpose of the present discussion is not a microscopic derivation of an effective $E2$ operator in nuclei with two valence nucleons but rather the use of effective charges determined from the two-nucleon $E2$ data in nuclei with $n > 2$ valence nucleons.

A. State-dependent effective charges

In this approach, the $E2$ operator remains of one-body character but state-dependent effective charges are taken. To distinguish this operator from the one with a constant effective charge, $\hat{T}_1(E2)$, it is denoted in the following as $\hat{T}'_1(E2)$. The idea is that, if the $B(E2; J \to J-2)$ values in the two-nucleon system cannot be explained with a constant effective charge, these can be made J dependent so as to reproduce the data. These effective charges are subsequently propagated to the n-nucleon systems. In Refs. [14,43,44] this procedure was applied to express $B(E2)$ values in the three-nucleon system in terms of those in the two-nucleon system. This could be achieved analytically under the assumption of conservation of seniority. In this subsection, we outline the procedure for n nucleons for a general interaction in a single-j orbital. In the next subsection analytic results are presented for an interaction that conserves seniority.

The matrix element of a one-body tensor of rank λ between n-body states can be calculated with the following recursive formula [45,46]:

$$\begin{aligned}\langle j^n \alpha' J' \| \hat{T}_1(\lambda) \| j^n \alpha J \rangle &= \frac{n}{n-1}(-)^{j+J}[J][J'] \sum_{\tilde{\alpha} R \tilde{\alpha}' R'} c^{\tilde{\alpha} R}_{n \alpha J} c^{\tilde{\alpha}' R'}_{n \alpha' J'} \\ &\times \begin{Bmatrix} J & J' & \lambda \\ R' & R & j \end{Bmatrix} \langle j^{n-1} \tilde{\alpha}' R' \| \hat{T}_1(\lambda) \| j^{n-1} \tilde{\alpha} R \rangle, \end{aligned} \tag{9}$$

where $[x] \equiv \sqrt{2x+1}$. The label α denotes possible quantum numbers needed to distinguish states of the j^n configuration with the same angular momentum J and $c^{\tilde{\alpha} R}_{n \alpha J}$ is a short-hand notation for the coefficient of fractional parentage $[j^{n-1}(\tilde{\alpha} R) j J | \} j^n \alpha J]$. Usually this recursion relation is applied until one arrives on the right-hand side at a one-nucleon matrix element, i.e., until $n = 2$. Therefore, for the operator $\hat{T}_1(E2)$ with a constant effective charge $e_{\rm eff}$, all $E2$ matrix elements between n-nucleon states can be expressed in terms of

$$\langle j \| \hat{T}_1(E2) \| j \rangle \equiv e_{\rm eff} \langle j \| r^2 Y_2 \| j \rangle = \sqrt{5} \tilde{e}_{\rm eff}, \tag{10}$$

where $\tilde{e}_{\rm eff}$ is proportional to the effective charge, $\tilde{e}_{\rm eff} = f_j(A) e_{\rm eff}$, with

$$f_j(A) = -\left(N + \frac{3}{2}\right) b^2 \left[\frac{(2j-1)(2j+1)(2j+3)}{64\pi j(j+1)} \right]^{1/2}. \tag{11}$$

For the operator $\hat{T}'_1(E2)$, with effective charges that depend on the two-nucleon states $|j^2 J\rangle$, the recursive procedure is halted when one arrives on the right-hand side of Eq. (9) at a *two*-nucleon matrix element

$$\begin{aligned}&\langle j^2 J_{\rm f} \| \hat{T}'_1(E2) \| j^2 J_{\rm i} \rangle \\ &\quad = -\sqrt{20}[J_{\rm f}][J_{\rm i}] \begin{Bmatrix} j & j & 2 \\ J_{\rm f} & J_{\rm i} & j \end{Bmatrix} \tilde{e}_{\rm eff}(J_{\rm i}, J_{\rm f}). \end{aligned} \tag{12}$$

This recursive procedure can only be carried out if all two-nucleon matrix elements, that is, all effective charges $\tilde{e}_{\rm eff}(J_{\rm i}, J_{\rm f})$, are known. If these are to be obtained from measured $E2$ data, that is unlikely to be possible since it would require the knowledge of the 'moment' effective charges $\tilde{e}_{\rm eff}(J_{\rm i}, J_{\rm f})$ with $J_{\rm i} = J_{\rm f}$. A possible strategy to circumvent this problem was outlined in Ref. [14] and leads to the following relation between $\tilde{e}_{\rm eff}(J, J)$ and $\tilde{e}_{\rm eff}(J, J-2)$:

$$\frac{\tilde{e}_{\rm eff}(J, J)}{\tilde{e}_{\rm eff}(J, J-2)} = \frac{[J]}{[J-2]} \begin{Bmatrix} j & j & 2 \\ J & J & j \end{Bmatrix} \begin{Bmatrix} j & j & 2 \\ J-2 & J & j \end{Bmatrix}^{-1}, \tag{13}$$

which allows to deduce all required effective charges from the $B(E2; J \to J-2)$ values in the nucleus with two nucleons in the valence space.

B. Analytic results for seniority-conserving interactions

As shown many years ago by de-Shalit and Talmi [45,46], the interaction between identical nucleons conserves seniority to a good approximation. With this assumption it is possible to derive analytic results for the matrix elements of $\hat{T}'_1(E2)$ between all states in a single-j orbital as long as $j \leqslant 9/2$, that is, if all states are uniquely defined by their angular momentum and seniority. The matrix elements of the one-body operator with state-dependent effective charges can be written in generic form as

$$\begin{aligned}&\langle j^n \upsilon_{\rm f} J_{\rm f} \| \hat{T}'_1(E2) \| j^n \upsilon_{\rm i} J_{\rm i} \rangle \\ &\quad = \sum_{J=2,4,\ldots}^{2j-1} f_J(j^n \upsilon_{\rm i} J_{\rm i} \upsilon_{\rm f} J_{\rm f}) \tilde{e}_{\rm eff}(J, J-2), \end{aligned} \tag{14}$$

where $f_J(j^n \upsilon_{\rm i} J_{\rm i} \upsilon_{\rm f} J_{\rm f})$ are numerical coefficients. Similar results relating the $B(E2)$ values in $n = 3$ and $n = 2$ nuclei were derived in Refs. [14,43] for $j = 7/2, 9/2$. The coefficients $f_J(j^n \upsilon_{\rm i} J_{\rm i} \upsilon_{\rm f} J_{\rm f})$ can be derived for any n and are available on request [47].

C. Application to $N = 50$ isotones

We apply the method outlined in the previous subsections to $N = 50$ isotones, making use of the complete set of $B(E2)$ values for the sequence $8_1^+ \to 6_1^+ \to 4_1^+ \to 2_1^+ \to 0_1^+$ measured in ^{92}Mo in order to fix an effective $E2$ operator. Similarly, an effective Hamiltonian appropriate for the $0g_{9/2}$ orbital can be derived from energy spectra. The two-body interaction matrix elements are taken from ^{92}Mo and from ^{98}Cd, corresponding to two valence particles and two valence

TABLE III. Experimental and calculated $B(E2)$ values in ^{93}Tc.

				$B(E2; J_i^\pi \to J_f^\pi)$ (e^2 fm^4)		
υ_i	J_i^π	υ_f	J_f^π	Exp	$\hat{T}_1(E2)$	$\hat{T}_1'(E2)$
3	$3/2_1^+$	3	$5/2_1^+$	–	212	256^{+7}_{-6}
3	$3/2_1^+$	3	$7/2_1^+$	–	31	35(1)
3	$5/2_1^+$	3	$7/2_1^+$	–	17	$9.0^{+1.3}_{-1.1}$
3	$5/2_1^+$	1	$9/2_1^+$	–	93	156(6)
3	$7/2_1^+$	1	$9/2_1^+$	–	178	278^{+9}_{-8}
3	$9/2_2^+$	3	$5/2_1^+$	–	23	32(1)
3	$9/2_2^+$	3	$7/2_1^+$	–	20	26(2)
3	$9/2_2^+$	1	$9/2_1^+$	–	11	16.0(5)
3	$9/2_2^+$	3	$11/2_1^+$	–	85	99(1)
3	$9/2_2^+$	3	$13/2_1^+$	–	3.3	4.8(3)
3	$11/2^+$	3	$7/2_1^+$	–	39	63(2)
3	$11/2_1^+$	1	$9/2_1^+$	–	59	87(3)
3	$11/2_1^+$	3	$13/2_1^+$	–	102	132(3)
3	$13/2_1^+$	1	$9/2_1^+$	–	102	166(6)
3	$15/2_1^+$	3	$11/2_1^+$	–	52	62(1)
3	$15/2_1^+$	3	$13/2_1^+$	–	16	$17.7^{+0.4}_{-0.3}$
3	$17/2_1^+$	3	$13/2_1^+$	88(18)[a]	99	114(3)
3	$17/2_1^+$	3	$15/2_1^+$	–	30	30.1(5)
3	$21/2_1^+$	3	$17/2_1^+$	73(5)[b]	57	61(1)

[a]From Ref. [48].
[b]From Ref. [49].

TABLE IV. Experimental and calculated $B(E2)$ values in ^{94}Ru.

				$B(E2; J_i^\pi \to J_f^\pi)$ (e^2 fm^4)		
υ_i	J_i^π	υ_f	J_f^π	Exp	$\hat{T}_1(E2)$	$\hat{T}_1'(E2)$
4	0_2^+	2	2_1^+	–	30	37(1)
4	0_2^+	4	2_2^+	–	128	164(4)
2	2_1^+	0	0_1^+	165(80)[a]	136	186(4)
4	2_2^+	0	0_1^+	–	7×10^{-6}	$0.07^{+0.06}_{-0.03}$
4	3_1^+	2	2_1^+	–	9×10^{-6}	$0.04^{+0.03}_{-0.02}$
4	3_1^+	4	2_2^+	–	66	79(1)
4	3_1^+	2	4_1^+	–	55	73(2)
4	3_1^+	4	4_2^+	–	12	14(1)
2	4_1^+	2	2_1^+	38(3)[a], 103(24)[b]	12	7.8(7)
2	4_1^+	4	2_2^+	–	25	35(1)
4	4_2^+	2	2_1^+	–	165	224(5)
4	4_2^+	4	2_2^+	–	9.5	15(1)
4	5_1^+	4	3_1^+	–	16	22(1)
4	5_1^+	2	4_1^+	–	124	173(4)
4	5_1^+	4	4_2^+	–	8.3	$5.4^{+0.4}_{-0.3}$
4	5_1^+	2	6_1^+	–	26	38(1)
4	5_1^+	4	6_2^+	–	16	23(1)
2	6_1^+	2	4_1^+	3.0(2)[b]	8.0	$3.9^{+0.5}_{-0.4}$
2	6_1^+	4	4_2^+	–	60	80(2)
4	6_2^+	2	4_1^+	–	25	36(1)
4	6_2^+	4	4_2^+	–	107	130^{+3}_{-2}
2	8_1^+	2	6_1^+	0.09(1)[b]	3.2	1.0(2)
2	8_1^+	4	6_2^+	–	98	137(3)
4	8_2^+	2	6_1^+	–	61	82(2)
4	8_2^+	4	6_2^+	–	21	27(1)
4	10_1^+	2	8_1^+	–	105	147(3)
4	10_1^+	4	8_2^+	–	22	23.3(4)

[a]From Ref. [5].
[b]From Ref. [13].

holes in $0g_{9/2}$, respectively, and an interpolated interaction is taken for intermediate $N = 50$ isotones. This procedure breaks particle-hole symmetry in the $0g_{9/2}$ orbital, akin to the effect of a three-body interaction. However, the interaction remains of two-body character and exhibits selection rules associated with the partial conservation of seniority, in particular in the midshell nucleus ^{95}Rh.

In the following we compare the results obtained with the operator $\hat{T}_1(E2)$ with a constant effective charge with those of the operator $\hat{T}_1'(E2)$ with state-dependent effective charges, and with the data when available. The input data depend on the assumed character of the $E2$ operator, as is explained below.

Results obtained with the two different $E2$ operators are summarised in Tables II–V for ^{92}Mo, ^{93}Tc, ^{94}Ru, and ^{95}Rh, respectively. Note that the method allows to estimate the uncertainty on a given $B(E2)$ value. For example, in the calculation with the operator $\hat{T}_1'(E2)$, one obtains information on how the uncertainties on the experimental values in the $n = 2$ nucleus ^{92}Mo propagate into the results for nuclei with $n > 2$.

We now comment on the results obtained with the two $E2$ operators.

1. The E2 operator with a constant effective charge

The effective charge derived from the quadrupole moment of the ground state of ^{91}Nb, $e_{\rm eff} = 1.32(16)$, is assumed to be normally, and therefore symmetrically, distributed around a central value. As a result all calculated $B(E2)$ values have asymmetric uncertainties—a property of the squared normal distribution. In this example it leads to an upper uncertainty of about 27% and a lower uncertainty that is somewhat smaller, 22%, uncertainties not indicated in the column labeled '$\hat{T}_1(E2)$' of Tables II to V.

Although calculations have been performed with a general two-body interaction, which in principle can break seniority symmetry for a $j = 9/2$ orbital, it is found that the υ quantum number is conserved to a very good approximation and for many states this conservation of seniority is rigorously valid. Specifically, in the midshell nucleus ^{95}Rh no mixing can occur between levels that differ by $\Delta\upsilon = 2$ [7,51] and therefore all levels carry an exact seniority quantum number with the exception of $9/2_1^+$, which is dominantly $\upsilon = 1$ but does carry a small $\upsilon = 5$ component, and $9/2_3^+$, which is orthogonal to it.

TABLE V. Experimental and calculated $B(E2)$ values in ^{95}Rh.

				$B(E2; J_i^\pi \to J_f^\pi)$ (e^2 fm^4)		
υ_i	J_i^π	υ_f	J_f^π	Exp	$\hat{T}_1(E2)$	$\hat{T}_1'(E2)$
5	$1/2_1^+$	3	$3/2_1^+$	–	161	205(4)
5	$1/2_1^+$	1	$5/2_1^+$	–	0	$0.98^{+0.24}_{-0.21}$
5	$1/2_1^+$	3	$5/2_2^+$	–	231	294(5)
3	$3/2_1^+$	1	$5/2_1^+$	–	10	13.1(2)
3	$3/2_1^+$	3	$5/2_2^+$	–	0	$1.5^{+0.5}_{-0.4}$
3	$3/2_1^+$	3	$7/2_1^+$	–	0	$0.61^{+0.24}_{-0.17}$
1	$5/2_1^+$	3	$7/2_1^+$	–	328	417^{+8}_{-7}
1	$5/2_1^+$	1	$9/2_1^+$	–	0	$0.04^{+0.03}_{-0.02}$
3	$5/2_2^+$	1	$5/2_1^+$	–	205	260(5)
3	$5/2_2^+$	3	$7/2_1^+$	–	0	$0.78^{+0.16}_{-0.14}$
3	$5/2_2^+$	1	$9/2_1^+$	–	125	159(3)
3	$7/2_1^+$	1	$9/2_1^+$	–	238	303^{+6}_{-5}
3	$11/2_1^+$	3	$7/2_1^+$	–	0	$0.02^{+0.03}_{-0.01}$
3	$11/2_1^+$	1	$9/2_1^+$	–	78	100(2)
5	$11/2_2^+$	3	$7/2_1^+$	–	97	123(2)
5	$11/2_2^+$	1	$9/2_1^+$	–	0	$0.05^{+0.04}_{-0.02}$
3	$13/2_1^+$	1	$9/2_1^+$	–	137	174(3)
3	$13/2_1^+$	3	$11/2_1^+$	–	0	$0.38^{+0.07}_{-0.06}$
3	$15/2_1^+$	3	$13/2_1^+$	–	0	<0.02
5	$15/2_2^+$	3	$13/2_1^+$	–	15	18.9(3)
3	$17/2_1^+$	3	$13/2_1^+$	–	0	$0.87^{+0.22}_{-0.19}$
3	$17/2_1^+$	3	$15/2_1^+$	–	0	$0.36^{+0.06}_{-0.05}$
5	$17/2_2^+$	3	$13/2_1^+$	–	168	213(4)
5	$17/2_2^+$	3	$15/2_1^+$	–	62	79(1)
3	$21/2_1^+$	3	$17/2_1^+$	24(2)[a]	0	1.0(2)
3	$21/2_1^+$	5	$17/2_2^+$	113(13)[a]	138	176(3)
5	$25/2_1^+$	3	$21/2_1^+$	–	86	109(2)

[a]From Ref. [50].

In ^{94}Ru, 4_2^+ and 2_2^+ are solvable states and carry exact $\upsilon = 4$ for any two-body interaction [52–54]. Furthermore, the usual selection rules hold for the one-body operator $\hat{T}_1(E2)$, namely the seniorities of the initial and final states cannot differ by more than 2, $\Delta\upsilon \leqslant 2$, and $E2$ transitions with $\Delta\upsilon = 0$ are suppressed toward, and exactly forbidden in, the middle of the orbital. As a result many $E2$ transitions in ^{95}Rh are therefore characterized by an exact '0' in the column '$\hat{T}_1(E2)$' of Table V. In the $n = 4$ nucleus ^{94}Ru the $\Delta\upsilon = 0$ $E2$ transitions are not exactly zero but rather suppressed. The only $\Delta\upsilon = 4$ transition in this nucleus is between 2_2^+ and 0_1^+, which is forbidden if seniority is conserved. The calculated result for the $2_2^+ \to 0_1^+$ transition in Table IV indicates that a very small breaking of seniority occurs in ^{94}Ru. Another transition with a tiny $B(E2)$ value is $3_1^+ \to 2_1^+$. The latter transition is forbidden if seniority is conserved due to a summation property of coefficients of fractional parentage.

2. The E2 operator with state-dependent effective charges

The state-dependent effective charges needed to reproduce the $B(E2; J \to J-2)$ values in ^{92}Mo are $e_{\rm eff}(J, J-2) = 1.99(6)$, 1.48(4), 1.39(2), and 1.31(1) for $J = 2$, 4, 6, and 8, respectively. These are obtained from $\tilde{e}_{\rm eff}(J, J-2) = f_j(A) e_{\rm eff}(J, J-2)$, where $f_j(A)$ is the proportionality factor defined in Eq. (11), together with the expressions

$$
\begin{aligned}
B(E2; 2_{\upsilon=2}^+ \to 0_{\upsilon=0}^+) &= \tfrac{2}{5}\tilde{e}_{\rm eff}(2,0)^2,\\
B(E2; 4_{\upsilon=2}^+ \to 2_{\upsilon=2}^+) &= \tfrac{91}{198}\tilde{e}_{\rm eff}(4,2)^2,\\
B(E2; 6_{\upsilon=2}^+ \to 4_{\upsilon=2}^+) &= \tfrac{500}{1573}\tilde{e}_{\rm eff}(6,4)^2,\\
B(E2; 8_{\upsilon=2}^+ \to 6_{\upsilon=2}^+) &= \tfrac{7}{55}\tilde{e}_{\rm eff}(8,6)^2. \qquad (15)
\end{aligned}
$$

The different values of the effective charge could also be an indication that there is more collectivity in the lowest transition, which could come from components with more than one $g_{9/2}$ pair, effectively coming from the excitations from $p_{1/2}$ [11,12] leading to mixing of configurations with different even number of protons in $g_{9/2}$, especially for the 0_1^+ state.

The $E2$ transition properties of the $N = 50$ isotones calculated with an $E2$ operator with state-dependent effective charges are shown in the column '$\hat{T}_1'(E2)$' of Tables II to V. All $B(E2)$ values in nuclei with $n \geqslant 3$ valence protons in the $0g_{9/2}$ orbital are expressed in terms of the two-nucleon effective charges $\tilde{e}_{\rm eff}(J, J-2)$ and do not depend on the one-nucleon effective charge $\tilde{e}_{\rm eff}$. Understandably, the effective charges $\tilde{e}_{\rm eff}(J, J-2)$ for $J = 6$ and 8 are close to $\tilde{e}_{\rm eff}$ derived from the quadrupole moment of the ground state of ^{91}Nb but $\tilde{e}_{\rm eff}(2, 0)$ is considerably and $\tilde{e}_{\rm eff}(4, 2)$ somewhat larger than $\tilde{e}_{\rm eff}$. This reflects the deviations for the $B(E2; 2_1^+ \to 0_1^+)$ and $B(E2; 4_1^+ \to 2_1^+)$ values in ^{92}Mo obtained with the operator $\hat{T}_1(E2)$ with a constant effective charge. As a result, most $B(E2)$ values calculated with state-dependent effective charges are larger than the corresponding ones obtained with a single effective charge. However, the differences cannot be represented by a simple scale factor. Generally, the $E2$ transitions between high angular momentum states do not change much while $B(E2)$ values between states of low angular momentum states do.

Two $B(E2)$ values have been measured to date in ^{93}Tc. The $B(E2; 21/2_1^+ \to 17/2_1^+)$ value essentially depends only on the effective charges $\tilde{e}_{\rm eff}(6, 4)$ and $\tilde{e}_{\rm eff}(8, 6)$ (see Table IV of Ref. [14]) and therefore is rather close to the value obtained with the $\hat{T}_1(E2)$ operator with a constant effective charge. The $B(E2; 17/2_1^+ \to 13/2_1^+)$ value depends additionally on the effective charge $\tilde{e}_{\rm eff}(4, 2)$, which leads to an increase compared with the result obtained with $\hat{T}_1(E2)$.

To obtain an understanding of the results for the nucleus ^{94}Ru in Table IV, we note that, under the assumption of seniority conservation, the relevant expressions for the $B(E2)$ values of the $6_1^+ \to 4_1^+$ and $8_1^+ \to 6_1^+$ transitions can be

derived from the matrix elements

$$\langle j^4 4^+_{\upsilon=2} \| \hat{T}'_1(E2) \| j^4 6^+_{\upsilon=2} \rangle = \sqrt{\frac{1}{5}} \left(-\frac{40}{33} \tilde{e}_{\rm eff}(2,0) + \frac{24220}{51909} \tilde{e}_{\rm eff}(4,2) + \frac{90422}{51909} \tilde{e}_{\rm eff}(6,4) + \frac{816}{1573} \tilde{e}_{\rm eff}(8,6) \right),$$

$$\langle j^4 6^+_{\upsilon=2} \| \hat{T}'_1(E2) \| j^4 8^+_{\upsilon=2} \rangle = \sqrt{\frac{119}{55}} \left(-\frac{526}{1485} \tilde{e}_{\rm eff}(2,0) + \frac{21046}{70785} \tilde{e}_{\rm eff}(4,2) - \frac{31604}{1061775} \tilde{e}_{\rm eff}(6,4) + \frac{13513}{32175} \tilde{e}_{\rm eff}(8,6) \right). \quad (16)$$

The calculated $B(E2)$ values in ^{94}Ru are obtained by inserting the state-dependent effective charges obtained from ^{92}Mo. Compared with the calculation with a constant effective charge a somewhat better agreement with the measured $B(E2)$ values is found but the improvement is marginal.

On the other hand, a disagreement is seen to occur for the $4^+_1 \to 2^+_1$ transition in ^{94}Ru. While the two experimental $B(E2; 4^+_1 \to 2^+_1)$ values are discrepant, both are significantly larger than the theoretical prediction. To obtain an understanding of this disagreement, it is essential to consider two 4^+ levels, which for four particles or four holes in a $j = 9/2$ orbital occur close in energy. For a one-body $E2$ operator with a constant effective charge the $B(E2)$ values in a $j = 9/2$ orbital, under the assumption of conservation of seniority, are

$$B(E2; 4^+_{\upsilon=2} \to 2^+_{\upsilon=2}) = \tfrac{91}{1782} \tilde{e}^2_{\rm eff},$$
$$B(E2; 4^+_{\upsilon=4} \to 2^+_{\upsilon=2}) = \tfrac{34000}{46629} \tilde{e}^2_{\rm eff}. \quad (17)$$

In ^{94}Ru (as well as ^{96}Pd) the dominant component of the 4^+_1 (4^+_2) state has seniority $\upsilon = 2$ ($\upsilon = 4$). Given that the $\Delta\upsilon = 2$ transition is ∼14 times faster than the one with $\Delta\upsilon = 0$, a small admixture of $\upsilon = 4$ in the 4^+_1 state can considerably alter the $B(E2; 4^+_1 \to 2^+_1)$ value. However, as has been shown in Refs. [52,53], the $4^+_{\upsilon=4}$ state is solvable for *any* interaction in a $j = 9/2$ orbital, which means that it cannot mix with other 4^+ states. A proper description of the $4^+_1 \to 2^+_1$ transition in ^{94}Ru and ^{96}Pd therefore necessarily must involve components outside the $0g_{9/2}$ orbital.

The use of a one-body $E2$ operator with state-dependent effective charges does not alter this conclusion. Under the assumption of seniority conservation, the matrix elements of the operator $\hat{T}'_1(E2)$ for $4^+ \to 2^+$ transitions in ^{94}Ru are

$$\langle j^4 2^+_{\upsilon=2} \| \hat{T}'_1(E2) \| j^4 4^+_{\upsilon=2} \rangle = \sqrt{\frac{7}{286}} \left(\frac{442}{165} \tilde{e}_{\rm eff}(2,0) - \frac{2369}{605} \tilde{e}_{\rm eff}(4,2) - \frac{12392}{9075} \tilde{e}_{\rm eff}(6,4) - \frac{476}{275} \tilde{e}_{\rm eff}(8,6) \right),$$

$$\langle j^4 2^+_{\upsilon=2} \| \hat{T}'_1(E2) \| j^4 4^+_{\upsilon=4} \rangle = \sqrt{\frac{85}{5181}} \left(\frac{446}{99} \tilde{e}_{\rm eff}(2,0) + \frac{1828}{363} \tilde{e}_{\rm eff}(4,2) + \frac{18802}{5445} \tilde{e}_{\rm eff}(6,4) + \frac{1156}{165} \tilde{e}_{\rm eff}(8,6) \right). \quad (18)$$

If one makes the association $4^+_1 = 4^+_{\upsilon=2}$ and $2^+_1 = 2^+_{\upsilon=2}$, one finds, with the effective charges obtained in ^{92}Mo, $B(E2; 4^+_1 \to 2^+_1) = 7.8(7)\ e^2\,{\rm fm}^4$, more than an order of magnitude smaller than observed in ^{94}Ru. In fact, with state-dependent effective charges the disagreement increases as compared to the result obtained with a constant effective charge.

While a single-j calculation cannot reproduce the observed $4^+_1 \to 2^+_1$ $E2$ transition in ^{94}Ru, at least not with reasonable effective charges, it can give insight into the problem by assuming an ad hoc mixed structure of the 4^+_1 state,

$$|4^+_1\rangle = \alpha_4 |4^+_{\upsilon=2}\rangle + \beta_4 |4^+_{\upsilon=4}\rangle \quad (19)$$

with $\alpha_4^2 + \beta_4^2 = 1$. A large $B(E2; 4^+_1 \to 2^+_1)$ value, as in ^{94}Ru, is obtained through a constructive interference between the two components, which happens if α_4 and β_4 have the opposite sign. The corresponding transition in ^{96}Pd is much slower [$B(E2; 4^+_1 \to 2^+_1) = 3.8(4)\ e^2\,{\rm fm}^4$] because of destructive interference: the $\Delta\upsilon = 0$ matrix elements change sign under particle-hole conjugation while those with $\Delta\upsilon = 2$ do not. This is the essence of the argument presented in Ref. [13], which therefore can be understood from a simple perspective.

It should be emphasized that, due to the dominance of the $\Delta\upsilon = 2$ over the $\Delta\upsilon = 0$ $E2$ transitions in ^{94}Ru, results are extremely dependent on the admixture β_4. In addition, since $6^+_{\upsilon=4}$ is also a solvable state [52,53], the same type of mixing should be assumed for the 6^+_1 state,

$$|6^+_1\rangle = \alpha_6 |6^+_{\upsilon=2}\rangle + \beta_6 |6^+_{\upsilon=4}\rangle \quad (20)$$

with $\alpha_6^2 + \beta_6^2 = 1$. The three $E2$ transitions, $4^+_1 \to 2^+_1$, $6^+_1 \to 4^+_1$ and $8^+_1 \to 6^+_1$, depend on the 4^+ or 6^+ mixing, or on both. The $B(E2)$ values between the mixed 4^+ and 6^+ states can be calculated with the help of Eqs. (16) and (18) together

with

$$\langle j^4 4^+_{\upsilon=4} \| \hat{T}'_1(E2) \| j^4 6^+_{\upsilon=2} \rangle = \sqrt{\frac{238}{6123}} \left(\frac{9256}{5445} \tilde{e}_{\text{eff}}(2,0) + \frac{66608}{19965} \tilde{e}_{\text{eff}}(4,2) + \frac{371744}{299475} \tilde{e}_{\text{eff}}(6,4) + \frac{28832}{9075} \tilde{e}_{\text{eff}}(8,6) \right),$$

$$\langle j^4 4^+_{\upsilon=2} \| \hat{T}'_1(E2) \| j^4 6^+_{\upsilon=4} \rangle = \sqrt{\frac{2261}{843}} \left(-\frac{1372}{5445} \tilde{e}_{\text{eff}}(2,0) + \frac{3352}{259545} \tilde{e}_{\text{eff}}(4,2) - \frac{160228}{778635} \tilde{e}_{\text{eff}}(6,4) - \frac{6664}{23595} \tilde{e}_{\text{eff}}(8,6) \right),$$

$$\langle j^4 4^+_{\upsilon=4} \| \hat{T}'_1(E2) \| j^4 6^+_{\upsilon=4} \rangle = \sqrt{\frac{2470}{44117}} \left(\frac{952}{1089} \tilde{e}_{\text{eff}}(2,0) + \frac{1149253}{311454} \tilde{e}_{\text{eff}}(4,2) + \frac{18704}{11979} \tilde{e}_{\text{eff}}(6,4) + \frac{6881}{1573} \tilde{e}_{\text{eff}}(8,6) \right),$$

$$\langle j^4 6^+_{\upsilon=4} \| \hat{T}'_1(E2) \| j^4 8^+_{\upsilon=2} \rangle = \sqrt{\frac{19}{9273}} \left(\frac{556}{33} \tilde{e}_{\text{eff}}(2,0) + \frac{12104}{1573} \tilde{e}_{\text{eff}}(4,2) + \frac{315992}{23595} \tilde{e}_{\text{eff}}(6,4) + \frac{15776}{715} \tilde{e}_{\text{eff}}(8,6) \right). \quad (21)$$

With the state-dependent effective charges fixed from ^{92}Mo all experimental $E2$ transitions in ^{94}Ru can be exactly reproduced with the admixtures $(\alpha_4, \beta_4) = (0.854, -0.520)$ and $(\alpha_6, \beta_6) = (0.994, -0.111)$ if the the experimental $B(E2; 4^+_1 \to 2^+_1)$ value of 103(24) is adopted. If the experimental $B(E2; 4^+_1 \to 2^+_1)$ value is taken as 38(3), reasonable agreement is obtained with the admixtures $(\alpha_4, \beta_4) = (0.980, -0.204)$ and $(\alpha_6, \beta_6) = (0.994, -0.113)$. It can therefore be concluded that the currently known $E2$ data in ^{94}Ru are consistent with moderate to strong seniority mixing of the 4^+ levels and 6^+ states that are rather pure in seniority.

Also for ^{95}Rh the known $B(E2)$ values for the states of interest are scarce (see Table V) due to the fact that only the lifetime of the $21/2^+_1$ state is known, yielding $B(E2)$ values to the first two $17/2^+$ states. The prediction for the seniority forbidden transition to the first $17/2^+$ state is clearly not in agreement with the experimental findings. Also here a mixing between both states could be considered provided more is known on the decay of both $17/2^+$ states.

V. CONCLUSION

Lifetimes of excited states in ^{92}Mo were measured using the γ-γ fast-timing technique in two independent experiments. The lifetime of the first excited 4^+ state was measured with high accuracy. The experimental $B(E2)$ values calculated with the measured lifetimes were used to obtain state dependent effective charges for the single-j calculation with $j = 9/2$. Comparing the predicted $B(E2)$ values for ^{93}Tc with the scarce experimental data, one finds that the single-j prediction qualitatively reproduces the experimental data within 3σ of the experimental uncertainties. The discrepancy from the $B(E2)$ for $B(E2; 4^+_1 \to 2^+_1)$ in ^{94}Ru to the experimental value is quantitatively discussed in terms of an ad hoc mixing between $\upsilon = 2$ and $\upsilon = 4$ states, with the result that in this way the experimental data in ^{94}Ru is exactly reproduced using state-dependent effective charges. Since the data on lifetimes in ^{93}Tc, ^{94}Ru, and ^{95}Rh is yet to be completed, further experiments are planned to probe the results from the single-j calculation.

ACKNOWLEDGMENTS

We acknowledge the Deutsche Forschungsgemeinschaft (DFG) for the upgrade of the used germanium detectors under Grant No. INST 216/988-1 FUGG. M.L. acknowledges the financial support of the DFG under Grant No. JOL 391/18-1. J.J. acknowledges support by GANIL for an extended stay there. Support of the University of Cologne in operating the Tandem accelerator is acknowledged.

[1] G. Racah, Phys. Rev. **63**, 367 (1943).
[2] R. Gross and A. Frenkel, Nucl. Phys. A **267**, 85 (1976).
[3] L. Coraggio *et al.*, J. Phys. G: Nucl. Part. Phys. **26**, 1697 (2000).
[4] J. Blomqvist and L. Rydström, Phys. Scr. **31**, 31 (1985).
[5] R. M. Pérez-Vidal *et al.*, Phys. Rev. Lett. **129**, 112501 (2022).
[6] J. J. Ressler *et al.*, Phys. Rev. C **69**, 034317 (2004).
[7] R. D. Lawson, *Theory of the Nuclear Shell Model* (Clarendon Press, Oxford, 1980).
[8] D. J. Rowe and G. Rosensteel, Phys. Rev. Lett. **87**, 172501 (2001).
[9] G. Rosensteel and D. J. Rowe, Phys. Rev. C **67**, 014303 (2003).
[10] E. Caurier, M. Rejmund, and H. Grawe, Phys. Rev. C **67**, 054310 (2003).
[11] H. Grawe, in *The Euroschool Lectures on Physics with Exotic Beams, Vol. I*, edited by J. Al-Khalili and E. Roeckl (Springer, Berlin/Heidelberg, 2004), pp. 33–75.
[12] H. Mach *et al.*, Phys. Rev. C **95**, 014313 (2017).
[13] B. Das *et al.*, Phys. Rev. C **105**, L031304 (2022).
[14] V. Karayonchev *et al.*, Phys. Rev. C **99**, 024326 (2019).
[15] A. Harter *et al.*, Nucl. Instrum. Methods Phys. Res. A **1053**, 168356 (2023).
[16] V. Karayonchev *et al.*, Phys. Rev. C **95**, 034316 (2017).
[17] A. Harter *et al.*, Phys. Rev. C **106**, 024326 (2022).
[18] L. Knafla *et al.*, Phys. Rev. C **102**, 044310 (2020).
[19] M. Stoyanova *et al.*, Phys. Rev. C **100**, 064304 (2019).
[20] H. Mach *et al.*, Nucl. Instrum. Methods Phys. Res. A **280**, 49 (1989).
[21] J.-M. Régis *et al.*, Nucl. Instrum. Methods Phys. Res. A **622**, 83 (2010).
[22] B. Olsen and L. Boström, Nucl. Instrum. Methods **44**, 65 (1966).
[23] Z. Bay, Phys. Rev. **77**, 419 (1950).

[24] J.-M. Régis *et al.*, Nucl. Instrum. Methods Phys. Res. A **726**, 191 (2013).
[25] J.-M. Régis *et al.*, Nucl. Instrum. Methods Phys. Res. A **897**, 38 (2018).
[26] J.-M. Régis *et al.*, Nucl. Instrum. Methods Phys. Res. A **823**, 72 (2016).
[27] M. Martin, Nucl. Data Sheets **114**, 1497 (2013).
[28] L. Knafla *et al.*, Nucl. Instrum. Methods Phys. Res. A **1052**, 168279 (2023).
[29] T. Numao *et al.*, Nucl. Phys. A **305**, 163 (1978).
[30] C. M. Baglin, Nucl. Data Sheets **113**, 2187 (2012).
[31] F. R. Metzger, Phys. Rev. C **15**, 193 (1977).
[32] C. Gil, J. Phys. Soc. Jpn. **34**, 575 (1973).
[33] K. E. G. Löbner, Nucl. Phys. **58**, 49 (1964).
[34] O. Häusser *et al.*, Nucl. Phys. A **293**, 248 (1977).
[35] C. Lederer *et al.*, Nucl. Phys. A **169**, 449 (1971).
[36] L. Hannappel *et al.*, Nucl. Instrum. Methods **167**, 289 (1979).
[37] A. Ádám *et al.*, Nucl. Phys. A **180**, 587 (1972).
[38] S. Cochavi *et al.*, Phys. Rev. C **3**, 1352 (1971).
[39] L. I. Govor *et al.*, Phys. At. Nucl. **73**, 1289 (2010).
[40] T. Kibédi *et al.*, Nucl. Instrum. Methods Phys. Res. A **589**, 202 (2008).
[41] J. Blomqvist and A. Molinari, Nucl. Phys. A **106**, 545 (1968).
[42] M. W. Kirson, Nucl. Phys. A **781**, 350 (2007).
[43] P. Spagnoletti *et al.*, Phys. Rev. C **95**, 021302(R) (2017).
[44] V. Karayonchev *et al.*, Phys. Rev. C **106**, 044321 (2022).
[45] A. de Shalit and I. Talmi, *Nuclear Shell Theory* (Academic Press, New York, 1963).
[46] I. Talmi, *Simple Models of Complex Nuclei: The Shell Model and Interacting Boson Model* (Harwood, Chur, 1993).
[47] P. Van Isacker (unpublished).
[48] C. Broude *et al.*, Z. Phys. A **336**, 133 (1990).
[49] C. M. Baglin, Nucl. Data Sheets **112**, 1163 (2011).
[50] S. Basu, G. Mukherjee, and A. Sonzogni, Nucl. Data Sheets **111**, 2555 (2010).
[51] J. J. Valiente-Dobón *et al.*, Phys. Lett. B **816**, 136183 (2021).
[52] A. Escuderos and L. Zamick, Phys. Rev. C **73**, 044302 (2006).
[53] P. Van Isacker and S. Heinze, Phys. Rev. Lett. **100**, 052501 (2008).
[54] Y. Qian and C. Qi, Phys. Rev. C **98**, 061303(R) (2018).